Human Aldose Reductase: Rate Constants for a Mechanism Including Interconversion of Ternary Complexes by Recombinant Wild-Type Enzyme†

Charles E. Grimshaw,*,‡ Kurt M. Bohren,§ Chung-Jeng Lai,‡ and Kenneth H. Gabbay§

Whittier Diabetes Program, Department of Medicine, University of California, San Diego, La Jolla, California 92093-0983, and Molecular Diabetes and Metabolism Section, Departments of Pediatrics and Cell Biology, Baylor College of Medicine, Houston, Texas 77030

Received March 13, 1995; Revised Manuscript Received July 24, 1995⊗

ABSTRACT: We have used transient kinetic data for partial reactions of recombinant human aldose reductase and simulations of progress curves for D-xylose reduction with NADPH and for xylitol oxidation with $NADP^+$ to estimate rate constants for the following mechanism at pH 8.0: E ⇄ E·NADPH ⇄ *E·NADPH ⇄ *E·NADPH·RCHO ⇄ *E·$NADP^+$·RCH_2OH ⇄ *E·$NADP^+$ ⇄ E·$NADP^+$ ⇄ E. The mechanism includes kinetically significant conformational changes of the two binary E·nucleotide complexes which correspond to the movement of a crystallographically identified nucleotide-clamping loop involved in nucleotide exchange. The magnitude of this conformational clamping is substantial and results in a 100- and 650-fold lowering of the nucleotide dissociation constant in the productive *E·NADPH and *E·$NADP^+$ complexes, respectively. The transient reduction of D-xylose displays burst kinetics consistent with the conformational change preceding $NADP^+$ release (*E·$NADP^+$ → E·$NADP^+$) as the rate-limiting step in the forward direction. The maximum burst rate also displays a large deuterium isotope effect ($^Dk_{burst}$ = 3.6−4.1), indicating that hydride transfer contributes significantly to rate limitation of the sequence of steps up to and including release of xylitol. In the reverse reaction, no burst of NADPH production is observed because the hydride transfer step is overall 85% rate-limiting. Even so, the conformational change preceding NADPH release (*E·NADPH → E·NADPH) still contributes 15% to the rate limitation for reaction in this direction. The estimated rate constant for hydride transfer from NADPH to the aldehyde of D-xylose (130 s^{-1}) is only 5- to 10-fold lower than the corresponding rate constant determined for NADH-dependent carbonyl reduction catalyzed by lactate or liver alcohol dehydrogenase. Hydride transfer from alcohol to $NADP^+$ (0.6 s^{-1}), however, is at least 100- to 1000-fold slower than NAD^+-dependent alcohol oxidation mediated by these two enzymes, resulting in a bound-state equilibrium constant for aldose reductase which greatly favors the forward reaction. The proposed kinetic model provides a basic set of rate constants for interpretation of kinetic results obtained with aldose reductase mutants generated for the purpose of examining structure−function relationships of different components of the native enzyme.

Previous studies established that aldose reductase (AR)[1] follows a compulsory ordered mechanism, with NADPH and $NADP^+$ binding first and leaving last, respectively, from the free enzyme (Boghosian & McGuinness, 1981; Wermuth et al., 1982; Ryle & Tipton, 1985; Tanimoto et al., 1986). Steady-state kinetic methods initially suggested that the rate of $NADP^+$ release, or alternatively the enzyme conformational change that precedes $NADP^+$ release, limits the overall forward reaction under conditions of saturating aldehyde concentrations (Grimshaw et al., 1989, 1990b). A subsequent stopped-flow study of nucleotide binding to porcine AR provided direct evidence for isomerization of the binary E·$NADP^+$ complex preceding $NADP^+$ release and confirmed that this isomerization rate was, within experimental error, equal to V/E_t for aldehyde reduction (Kubiseski et al., 1992). Interpretation of these stopped-flow data relied on analysis of the nucleotide concentration dependence of a rather poorly defined "second phase" in a two-phase exponential transient, and no attempt was made to estimate the rate constants for formation and interconversion of the ternary central complexes where hydride transfer occurs.

In this study, we have used rapid reaction kinetic methods to analyze the binding of nucleotides to the free enzyme, single turnover progress curves for xylose reduction, and multiple turnover transients including the steady-state period for both xylose reduction and xylitol oxidation catalyzed by recombinant human aldose reductase (hAR). We have chosen an appropriate aldose substrate and product pair, namely D-xylose and xylitol, and have employed the natural cofactors, NADPH and $NADP^+$, in studying the reaction at pH 8.0 in both directions. The results described herein

† This work was supported by NIH Grants DK 43595 (C.E.G.) and EY 11018 (K.H.G.), Juvenile Diabetes Foundation grants (K.M.B. and K.H.G.), and the Harry B. and Aileen B. Gordon Foundation (K.H.G.).

* Address correspondence to this author, at the University of California, San Diego, Whittier Diabetes Program, Department of Medicine 0983, 9500 Gilman Dr., La Jolla, CA 92093-0983. Phone: (619) 535-8037 or (619) 622-8422 (new); Fax: (619) 535-0894; Internet: cgrimshw@scripps.edu.

‡ University of California, San Diego.

§ Baylor College of Medicine.

⊗ Abstract published in *Advance ACS Abstracts,* October 15, 1995.

[1] Abbreviations: Na_2EDTA, disodium ethylenediaminetetraacetate; $NADP^+$, β-nicotinamide adenine dinucleotide phosphate; NADPH, reduced form of $NADP^+$; AR, aldose reductase; hAR, recombinant human aldose reductase; NADPD, (4*R*)-[4-^{2}H]NADPH; DTT, dithiothreitol; LADH, liver alcohol dehydrogenase; LDH, lactate dehydrogenase; AlaDH, alanine dehydrogenase; ARI, aldose reductase inhibitor.

0006-2960/95/0434-14356$09.00/0

establish estimates for each of the rate constants in the overall reaction mechanism using both protio- and deuterio-NADPH. We also demonstrate novel burst kinetics for aldehyde reduction for this enzyme class and other findings which confirm and, in several instances, extend the conclusions of the previously published stopped-flow study (Kubiseski et al., 1992). We further show that the bound-state equilibrium constant for hAR strongly favors the forward reaction primarily because hydride transfer in the alcohol oxidation direction is unusually slow for an NAD(P)-dependent dehydrogenase. The complete kinetic model presented here provides the basis for better understanding of the mechanistic and functional roles of various structural domains and specific amino acid residues within the enzyme itself, as well as the kinetic behavior of various aldose reductase inhibitors.

MATERIALS AND METHODS

Materials. Recombinant human aldose reductase was prepared and purified as previously described (Bohren et al., 1991). Enzyme was stripped of all nucleotide using the method of Ehrig et al. (1994), and the protein concentration was estimated using $\epsilon^{280\ nm} = 48.2\ mM^{-1}\ cm^{-1}$, based on the known amino acid composition using published extinction coefficients for Trp ($5.69\ mM^{-1}\ cm^{-1}$) and Tyr ($1.28\ mM^{-1}\ cm^{-1}$) residues (Gill & von Hippel, 1989). Stereospecifically labeled (4*R*)-[4-^{2}H]NADPH (NADPD) was synthesized and purified as described (Bohren et al., 1992). D-xylose, xylitol, NADPH, and $NADP^+$ were purchased from Sigma, and the best available grades of other chemicals and biochemicals were used without further purification. Solutions were prepared using Milli-Q deionized water, and pH was measured with a Radiometer PHM 84 pH meter with a GK 2321C combined electrode.

Stopped-Flow Kinetic Studies. A Bio-Logic MPS-51 stopped-flow instrument equipped with MOS-1000 modular optical system including a 150W Hg-Xe lamp (absorbance and fluorescence detection), three syringes, a path length of 1 cm, and a dead time of 2 ms, along with Bio-Kine rapid kinetics data acquisition and analysis software, were used to obtain transient data and to calculate apparent first-order rate constants. Reactions were conducted at 25 °C in 33 mM sodium phosphate buffer (pH 8) containing 0.5 mM Na_2-EDTA and 0.1 mM DTT. For coenzyme binding experiments, the three syringes contained (1) coenzyme (NADPH or $NADP^+$), (2) buffer, and (3) enzyme (1.5 μM), respectively, in standard phosphate buffer. The final coenzyme concentration was varied by changing the relative volumes added from syringes 1 and 2, while keeping the total volume constant. Coenzyme binding was monitored as quenching of enzyme fluorescence (excitation: 294 nm, emission: 315−390 nm, combined glass + black interference filters). For measurement of single or multiple turnover transients, syringes contained the following: (1) coenzyme plus substrate, (2) coenzyme, and (3) enzyme (10−12.5 μM), respectively, in standard phosphate buffer. The final substrate concentration was varied in a similar manner by changing the relative volumes added from syringes 1 and 2, while keeping the final coenzyme concentration constant. Concentrations given in the tables and figures represent the final concentrations in the reaction mixtures. Reduction of xylose and oxidation of xylitol were monitored as the change in absorbance at 363 nm using extinction coefficients estimated for free ($\epsilon = 3.4\ mM^{-1}\ cm^{-1}$) and enzyme-bound ($\epsilon = 4.2\ mM^{-1}\ cm^{-1}$) NADPH.[2]

Initial Velocity Studies. Conventional steady-state initial velocities for hAR-mediated xylose reduction or xylitol oxidation were monitored as the rate of enzyme-dependent decrease or increase, respectively, in fluorescence of free NADPH ($_{340\ nm}F_{460\ nm}$; excitation and emission slits both 1.0 mm) using a Spex Fluoromax photon counting spectrofluorimeter equipped with xenon lamp and interfaced with an 80286 microcomputer. Assays were conducted in quartz 1.0-cm^2 cuvettes in a final volume of 3.0 mL of standard phosphate buffer. Reactions were routinely monitored for 2 min, and the digitized reaction time course was analyzed using the manufacturer's DM 3000F software package to obtain the initial slope ($\Delta F/\Delta t$). The instrument, calibrated each day using a known stock solution of NADPH, gave a linear response over the 0−10 μM NADPH concentration range. Fluctuations in lamp intensity were electronically corrected for by collecting data as the ratio of sample to reference intensity. All rates were corrected for any background rate (≤5%) detected in the absence of enzyme or substrate.

Data Processing. Values for microscopic rate constants were estimated by analysis of stopped-flow progress curves using the manual kinetic simulation program KINSIM (Barshop et al., 1983) and the automatic fitting routine FITSIM (Zimmerle et al., 1987) as modified for use under Windows 3.1 by Drs. Bryce V. Plapp and Gary X. Hua. The progress curves shown in the figures are the actual experimental data, while the curves are KINSIM simulations generated using the estimated rate constant values and the actual starting concentrations of enzyme, coenzyme, and substrate. The observed first-order rate constant (k_{obs}) for nucleotide binding (via a two-step mechanism, eq 5), as a function of the total nucleotide concentration (N_t) was fitted to:

$$k_{obs} = k_4 + k_3 f_{E\cdot Nucl} \quad (1)$$

where the fraction $f_{E\cdot Nucl} = (E\cdot Nucl/E_t)$ is given by:

$$f_{E\cdot Nucl} = (^1/_2E_t)\{(E_t + N_t + K_d) - [(E_t + N_t + K_d)^2 - 4E_tN_t]^{1/2}\} \quad (2)$$

and E_t is the total enzyme concentration, and $K_d = (k_2/k_1)$ is the dissociation constant for the initial E·Nucl complex (see Results). The minimum value of k_4 was set equal to the turnover number for reaction in that direction in order to obtain estimates for k_3 and K_d (see Results). In other cases where saturation behavior was observed, the maximum apparent rate constant (k_{max}) and half-saturation constant ($K_{1/2}$) were determined from fits of the experimental data for k as a function of the concentration of A:

$$k = k_{max}A/(K_{1/2} + A) \quad (3)$$

by the least-squares method, assuming equal variances for the k_{obs} values (Wilkinson, 1961) using the Hyper program of Cleland (1979). For initial velocity studies experimental

[2] A shift in λ_{max} from 340 nm for NADPH in solution to 355 nm in the *E·NADPH complex results in a greater extinction coefficient at 363 nm for the bound species, similar to that observed for the bovine enzyme (Grimshaw et al., 1990a).

Table 1: Rate and Equilibrium Constants for Nucleotide Binding to hAR

nucleotide	fitting method	K_d (μM)	k_1 (M^{-1} s^{-1})	k_2 (s^{-1})	k_3 (s^{-1})	k_4[a] (s^{-1})	K_i[b] (nM)	K_d/K_i
$NADP^+$	SigmaPlot	7.4 ± 2.7			176 ± 11	⟨0.20⟩	8	880
	Fitsim	3.1	(2.0 ± 0.1) × 10^8	623 ± 40	150 ± 6	0.23 ± 0.10	5	650
NADPH	SigmaPlot	2.3 ± 1.4			96 ± 19	⟨0.05⟩	1.2	1900
	Fitsim	1.5	(1.2 ± 0.1) × 10^8	174 ± 13	89 ± 3	0.83 ± 0.10	13	107

[a] Broken brackets contain steady-state $\langle V/E_t \rangle$ values for reaction in the opposite direction. [b] $K_i = k_2/k_1(1.0 + (k_3/k_4))$ is the dissociation constant for the tight complex *E·Nucl.

data were fitted to:

$$v_i = VAB/(K_{ia} + K_aB + K_bA + AB) \quad (4)$$

which describes a sequential initial velocity pattern, using the Sequen program of Cleland (1979). In eqs 3 and 4, A and B are the concentrations of substrates A and B, respectively, v_i is the initial velocity, V is the maximum velocity, K_{ia} is the dissociation constant for A, and K_a and K_b are the Michaelis constants for A and B, respectively.

RESULTS

Nucleotide Binding. Progress curves (quenching of enzyme fluorescence) for nucleotide binding to hAR were in all cases best fit using a single exponential (Figure 1); we saw no consistent evidence for a second slower phase using either $NADP^+$ or NADPH over a wide range of nucleotide concentration.[3] Plots of k_{obs} versus nucleotide concentration ([nucleotide]) displayed saturation behavior (inset, Figure 1), consistent with a two-step binding mechanism:

$$E + Nucl \underset{k_2}{\overset{k_1}{\rightleftharpoons}} E{\cdot}Nucl \underset{k_4}{\overset{k_3}{\rightleftharpoons}} {*}E{\cdot}Nucl \quad (5)$$

where E is hAR and Nucl is either NADPH or $NADP^+$. In eq 5, rapid formation of a weak initial E·Nucl complex is followed by a conformational change to a tightly bound, productive *E·Nucl complex, and the observed first-order rate constant is given by eqs 1 and 2. This kinetic model for nucleotide binding to hAR is consistent with the known crystallographic structure of the holoenzyme where nucleotide binding to the "open" enzyme (Rondeau et al., 1992) induces movement of the nucleotide enfolding loop to close, forming the tightly bound *E·Nucl binary complex (Wilson et al., 1992, 1993; Borhani et al., 1992; Harrison et al., 1994; Bohren et al., 1994). We considered and discarded other two-step binding models, such as a direct competition for free enzyme between productive and dead-end E·Nucl complex formation or a conformational change of the free enzyme followed by nucleotide binding, since the variation in the rate and magnitude of the observed fluorescence changes as a function of nucleotide concentration was not consistent with that predicted for alternative models (Grimshaw & Lai, 1995).

As a first approximation, data for k_{obs} as a function of nucleotide concentration were fitted to eqs 1 and 2 using as a lower limit for k_4, the V/E_t value determined from initial velocity measurements for reaction in the opposite direction

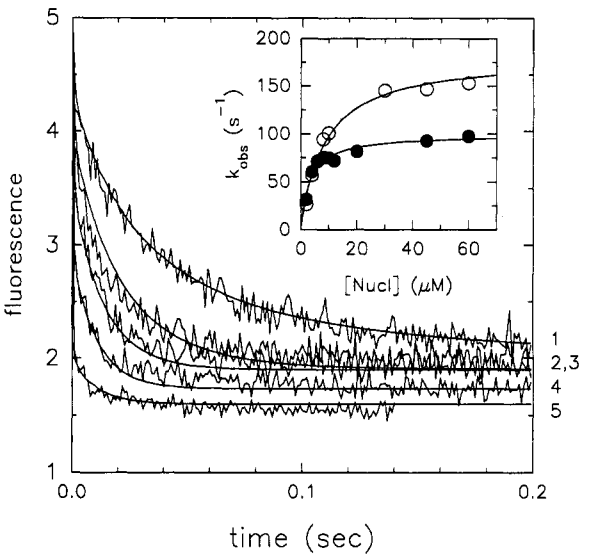

FIGURE 1: Stopped-flow progress curves for $NADP^+$ binding to hAR monitored as quenching of enzyme fluorescence ($_{294\ nm}F_{>315\ nm}$). Reactions in standard phosphate buffer contained 1.5 μM enzyme and the following concentrations of $NADP^+$: 2 μM (1); 4 μM (2); 6 μM (3); 10 μM (4); and 45 μM (5). Actual progress curves shown are averages of 3−4 kinetic transients; solid lines were calculated using rate constants (Table 1) determined for the two-step binding mechanism (eq 5) by KINSIM/FITSIM analysis of the entire data set for each nucleotide. First-order rate constants (k_{obs}) determined from Bio-Kine analysis of individual progress curves showed standard errors of 1% or better. Inset: Plots of k_{obs} versus nucleotide concentration with NADPH (●) and $NADP^+$ (○) show saturation kinetics; solid lines were calculated from fits of the k_{obs} data to eqs 1 and 2.

(since each rate constant along the pathway must be at least as large as the overall V/E_t). The results for k_3 and K_d are listed in Table 1. A second approach utilized least-squares analysis of the progress curves themselves, starting with estimates for each of the four rate constants in eq 5. This approach, which has been described in detail elsewhere (e.g., see Sekhar & Plapp, 1988), involved two steps. First, we chose reasonable values for each of the rate constants and simulated, using KINSIM, each in the series of progress curves obtained at a given nucleotide concentration. Next, we used visual comparison and overall error analysis to decide on which rate constant values best simulated the overall data set. The entire set of progress curves were then simultaneously analyzed by an iterative least-squares process using FITSIM to obtain the best fit rate constants for the entire data set. The robustness of each fit was evaluated by showing that similar final rate constant values were obtained when different initial estimates were used. As shown in Table 1, the derived values routinely displayed standard errors with values less than 20%, and the results obtained by the two different fitting procedures were in reasonable agreement.

[3] Detection of a second slow phase in the fluorescence quenching progress curve was a function of the enzyme sample used and could be correlated with the presence of contamination by the "oxidized" enzyme form (Srivastava et al., 1985; Grimshaw et al., 1989; Del Corso et al., 1989; Vander Jagt & Hunsaker, 1993; Bohren & Gabbay, 1993).

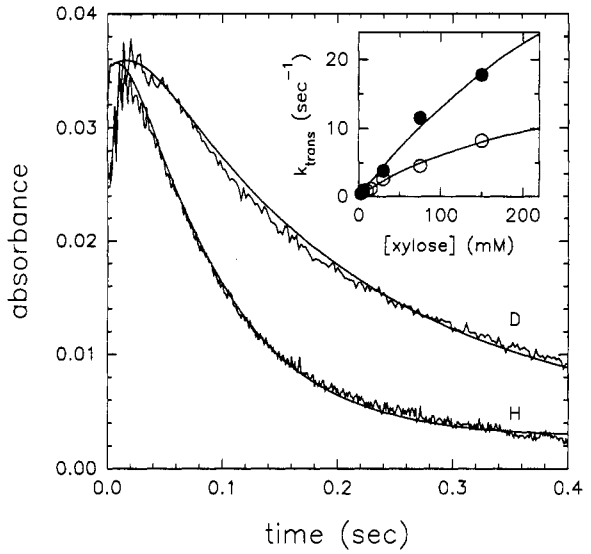

FIGURE 2: Single turnover stopped-flow progress curves for hAR-catalyzed D-xylose reduction monitored by absorbance change at 363 nm. Reactions in standard phosphate buffer contained 10 μM enzyme, 75 mM D-xylose, and 9 μM NADPH (H) or NADPD (D). Actual progress curves are shown; solid lines were calculated using rate constants determined for the complete mechanism (Scheme 1) by KINSIM/FITSIM analysis of the entire data set including progress curves for each nucleotide obtained at a range of D-xylose concentrations. First-order rate constants (k_{trans}) determined from Bio-Kine analysis of the $A_{363\ nm}$ decrease for individual progress curves showed standard errors of 4% or better. Inset: Plots of k_{trans} versus [xylose] with NADPH (●) and NADPD (○) show saturation kinetics.

In general, the weak initial E·Nucl complex displayed a K_d value in the micromolar range, while the tight complex showed a K_i value in the nanomolar range, representing a 100- to 650-fold tighter binding in the productive *E·Nucl complex. The k_4 value determined for $NADP^+$ is similar to V/E_t for xylose reduction consistent with *E·$NADP^+$ isomerization as the rate-limiting step for reaction in this direction. Our data also indicate that *E·NADPH isomerization does not limit the rate of xylitol oxidation. On the surface, these results are similar to those reported for the porcine enzyme; however, the magnitude of the other rate constants determined for hAR are significantly greater than those reported (Kubiseski et al., 1992). Presumably, this discrepancy derives from the limited nucleotide concentration range employed in the porcine enzyme study which precluded the clear demonstration of saturation behavior for nucleotide binding described here.

Single Turnover Experiments. Figure 2 shows a representative pair of single turnover progress curves measured using NADPH and NADPD as the nucleotide cofactor at 75 mM D-xylose. Such progress curves routinely displayed an increase in $A_{363\ nm}$ during the first 20−30 ms due to the shift in absorbance maximum for bound NADPH,[2] followed by a decrease in absorbance due to NADPH oxidation. The latter decrease in $A_{363\ nm}$ was in all cases best fit using a single exponential. A plot of the experimentally determined first-order rate constant (k_{trans}) derived from the kinetic transient versus D-xylose concentration ([D-xylose]) with either NADPH or NADPD displayed saturation kinetics (inset, Figure 2). A fit to eq 3 of the data for NADPH gave values of $k_{trans} = 76 \pm 58\ s^{-1}$ and $K_{xylose} = 480 \pm 460$ mM, while a similar fit for NADPD gave values of $k_{trans} = 21 \pm 6\ s^{-1}$ and $K_{xylose} = 244 \pm 100$ mM. The large standard errors

Scheme 1

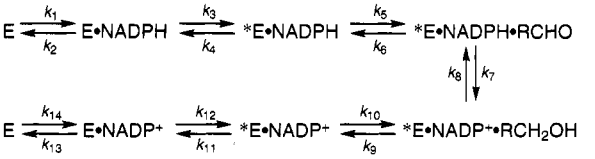

in k_{trans} and K_{xylose} result from the necessarily inexact extrapolation from a maximum experimental concentration of D-xylose concentration (150 mM) that was roughly half the estimated K_{xylose} value for reactions with NADPH (350 mM).[4] The k_{trans}/K_{xylose} ratios (analogous to $V/K_{xylose}E_t$, the first-order term for steady-state turnover at low concentrations of D-xylose) were, however, well-determined by the data with values of $158 \pm 31\ M^{-1}\ s^{-1}$ and $87 \pm 12\ M^{-1}\ s^{-1}$ for NADPH and NADPD, respectively. The fact that k_{trans} reaches saturation requires that there be a slow step either preceding or following xylose binding which becomes rate-limiting at infinite D-xylose concentration.[5] The presence of a significant primary deuterium isotope effect[6] on k_{trans} ($^Dk_{trans} = 3.6 \pm 2.9$) and k_{trans}/K_{xylose} ($^D(k_{trans}/K_{xylose}) = 1.81 \pm 0.44$), however, requires that hydride transfer make a substantial contribution to the rate limitation of the single turnover transient rate.

As was done for the nucleotide binding determinations, the entire set of progress curves for single turnover transient reduction of D-xylose with NADPH and NADPD was analyzed using KINSIM and FITSIM according to the complete reaction mechanism outlined in Scheme 1, where E is hAR, RCHO is D-xylose, RCH_2OH is xylitol, and *E is the isomerized form of the enzyme. Since these are single turnover experiments, only steps up to and including xylitol release (k_9) were included in the simulations. Values of $k_1 - k_4$ used were those determined from the NADPH binding studies. During the initial KINSIM/FITSIM analysis, fits to the progress curves were found to be insensitive to changes in k_9 and k_{10}. These rate constants were thus set at values high enough to be kinetically transparent, yet maintain a ratio (k_9/k_{10}) equal to the $K_{xylitol}$ value determined either by conventional steady-state kinetic methods or from the saturation kinetics observed for the linear phase of xylitol oxidation in multiple turnover experiments (see below). Similarly, the k_8 value was chosen such that the net rate constant (Cleland, 1975) for this step ($k_8' = k_8k_6/(k_6 + k_7)$) was equal to $V_{xylitol}/E_t$. Unfortunately, k_8 was not well-determined by these experiments, since $k_7 \gg k_8$. The best value for k_8 came from analysis of the xylitol oxidation progress curves. The results obtained from the KINSIM/FITSIM analysis are described below in the context of the multiple turnover studies.

Multiple Turnover ("Burst Kinetics") Experiments. When the NADPH concentration was increased to 140 μM to allow multiple turnovers, the progress curves for D-xylose reduction

[4] K_{xylose} estimated as $(k_{eff} + k_6)/k_5$, where $k_{eff} = [(1/k_7) + (1/k_3)]^{-1}$, is the effective rate constant for a single turnover transient at infinite xylose concentration, according to Scheme 1.

[5] Because preformed E·NADPH complex was not used, a slow step preceding (e.g., E·NADPH → *E·NADPH) or following (e.g., *E·NADPH·xylose → °E·NADPH·xylose) D-xylose binding could become rate-limiting for a single turnover transient at infinite D-xylose concentration.

[6] The isotope effect nomenclature used is that of Northrop (1977) and Cleland (1987) in which a leading superscript indicates the isotope effect being studied. Thus, ^DV, $^DV/K$, and ^Dk are primary deuterium isotope effects on V/E_t, V/KE_t, and k, respectively.

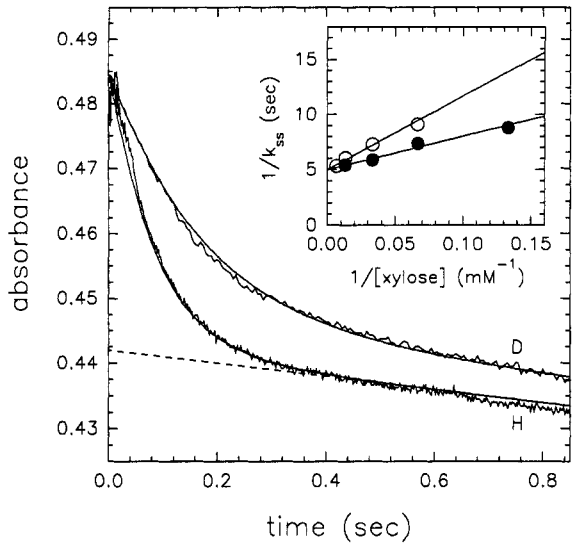

FIGURE 3: Multiple turnover stopped-flow progress curves for hAR-catalyzed D-xylose reduction. Reactions in standard phosphate buffer contained 12.5 μM enzyme, 75 mM D-xylose, and 140 μM NADPH (H) or NADPD (D). Actual progress curves shown emphasize the pre-steady-state burst; data were collected up to 10 s to establish the steady-state rate. The solid lines were calculated as described for Figure 2. The burst magnitude (-0.0425 ± 0.010 $A_{363\ nm}$) for NADPH (dashed line) corresponds to >0.99 enzyme equivalents. Inset: Double reciprocal plots of $1/k_{ss}$ versus 1/[D-xylose] with NADPH (●) and NADPD (○) show saturation kinetics for the linear, steady-state phase of the reaction.

displayed "burst kinetics" with an initial exponential decline in absorbance followed by a steady-state rate of NADPH disappearance (Figure 3). Progress curves were analyzed using the Bio-Kine software to obtain the absorbance change (ΔA_{burst}) and first-order rate constant (k_{burst}) for the burst phase, and the zero-order rate constant (k_{ss}) for the linear phase of the reaction. With NADPH, ΔA_{burst} was essentially constant (-0.0425 ± 0.010 $A_{363\ nm}$) over the xylose concentration range tested (7−150 mM), corresponding to a burst of 12.5 μM or >99% of the enzyme present.

Both k_{ss} (inset, Figure 3) and k_{burst} (not shown) displayed saturation kinetics with respect to D-xylose concentration, and fits of the data to eq 3 gave the following results. With NADPH, the burst phase showed $k_{burst} = 62 \pm 9$ s^{-1} and $K_{xylose} = 320 \pm 63$ mM, while the steady-state rate showed $k_{ss} = 0.20 \pm 0.02$ s^{-1} (equal to V_{xylose}/E_t) and $K_{xylose} = 6.1 \pm 2.4$ mM (equal to K_{xylose}).[7] With NADPD, the corresponding burst phase data showed $k_{burst} = 15 \pm 1$ s^{-1} and $K_{xylose} = 144 \pm 12$ mM, and the steady-state rate data showed $k_{ss} = 0.20 \pm 0.03$ s^{-1} and $K_{xylose} = 13 \pm 7$ mM. The calculated primary deuterium isotope effects derived from both the burst phase ($^Dk_{burst}$ and $^D(k_{burst}/K_{xylose})$) and linear phase ($^Dk_{ss}$ and $^D(k_{ss}/K_{xylose})$) rate data are compared in Table 2 with the corresponding values obtained from single turnover experiments ($^Dk_{trans}$ and $^D(k_{trans}/K_{xylose})$), and with those determined by the conventional method of direct comparison of initial velocities ($^DV_{xylose}$ and $^DV/K_{xylose}$). Unlike the case for D-xylose reduction, multiple turnover progress curves for xylitol oxidation displayed only a steady-state phase as shown by a linear appearance of NADPH absorbance with time (not shown). Fitting the k_{ss} data as a function of [D-xylitol] to eq 3 gave $k_{ss} = 0.07 \pm 0.02$ s^{-1} (equal to $V_{xylitol}/E_t$) and $K_{xylitol} = 200 \pm 30$ mM (equal to $K_{xylitol}$).

[7] A more accurate K_{xylose} value is obtained by conventional initial velocity studies using D-xylose concentrations from 0.2 to 5 times K_{xylose} (Table 4).

Table 2: Comparison of Calculated and Observed Primary Deuterium Isotope Effects on Xylose Reduction

measurement[a]	$^Dk_{max}$	$^D(k_{max}/K_{xylose})$
single turnover (k_{trans})	3.6 ± 2.9	1.81 ± 0.44
burst: multiple turnover (k_{burst})	4.1 ± 0.6	1.84 ± 0.12
burst: k_{burst} calcd from model[b]	3.23	1.89
stopped-flow steady state (k_{ss})	1.02 ± 0.12	2.2 ± 1.0
initial velocity (V_{xylose}/E_t)	1.00 ± 0.02	1.82 ± 0.05
calcd "intrinsic" effect: $^Dk_7 = (k_{7H}/k_{7D})$	6.50	

[a] All measurements in 33 mM phosphate buffer (pH 8.0) at 25 °C. [b] At saturating levels of NADPH and xylose, $k_{burst} = ((1/k_3) + (1/k_7))^{-1}$; thus, $^Dk_{burst} = (k_{burstH}/k_{burstD}) = (^Dk_7 + (k_{7H}/k_3))/(1.0 + (k_{7H}/k_3)) = (6.50 + 1.46)/(1.00 + 1.46) = 3.23$. At limiting D-xylose, $^D(k_{burst}/K_{xylose}) = (^Dk_7 + (k_{7H}/k_6))/(1.0 + (k_{7H}/k_6)) = 1.89$.

KINSIM/FITSIM analysis of the entire set of progress curves for multiple turnover experiments using both NADPH and NADPD served to further refine the values for k_5-k_8 derived from fitting the progress curves from single turnover experiments. Once again, the simulations were insensitive to large variations in the values of k_9 and k_{10}. The value of k_8, which was not well determined by the single turnover transient data, was limited to a narrow range by the $V_{xylitol}/E_t$ value determined for xylitol oxidation, and by the fact that the net rate constant corresponding to k_8 is at least 10-fold slower than any other step for reaction in this direction. However, because only one data set contributes significantly to the assignment of k_8, the absolute magnitude of this rate constant must be considered approximate at this time. Conversely, while the values for k_5-k_7 determined in each individual FITSIM analysis displayed standard errors up to 25%, the requirement that the kinetic model accurately reproduce the experimental results of four independent data sets (single or multiple turnover studies with NADPH or NADPD, respectively) placed rather narrow constraints on the values of these rate constants. Thus, only k_7 and k_8 were allowed to vary between the NADPH and NADPD data sets; rate constants for xylose binding and release (k_5 and k_6) were assumed to be the same for either nucleotide. The value shown for k_{8D} was estimated as $k_{8D} = (k_{8H}{}^DK_{eq}/^Dk_7)$, where $^Dk_7 = k_{7H}/k_{7D}$ was determined directly from progress curves with NADPH and NADPD and $^DK_{eq} = (k_{7H}/k_{8H})/(k_{7D}/k_{8D})$ is the equilibrium isotope effect for NAD(P)D-linked reduction of an aldehyde to a primary alcohol, $^DK_{eq} = 0.93$ (Cook et al., 1980). Table 3 contains a list of the estimated rate constants determined for the mechanism shown in Scheme 1.

Values of the observable kinetic parameters (e.g., V_{xylose}/E_t, K_{xylose}, etc.) were also calculated by substituting the estimated rate constants from Table 3 into kinetic expressions derived according to Scheme 1 (see supporting information). As shown in Table 4, the agreement between the measured and calculated values is quite good. As a further check on the internal consistency of the proposed kinetic model, the calculated K_{eq} value (6.7×10^{13} M^{-1}, based on the free carbonyl form of D-xylose (Hayward & Angyal, 1977)) was found to be in good agreement with the published values (average value of 5.2×10^{13} M^{-1}, based on free carbonyl form) for reduction of the α-hydroxyaldehydes, DL-glycer-

Table 3: Estimated Rate Constants for the Reactions of D-Xylose and Xylitol[a]

	forward		reverse
k_1	$1.2 \times 10^8\ M^{-1}\ s^{-1}$	k_2	$174\ s^{-1}$
k_3	$89\ s^{-1}$	k_4	$0.83\ s^{-1}$
k_5	$220\ M^{-1}\ s^{-1}$ [c]	k_6	$25\ s^{-1}$
k_7	$130\ s^{-1}$ ($20\ s^{-1}$)[b]	k_8	$0.60\ s^{-1}$ ($0.09\ s^{-1}$)[b]
k_9	$1.0 \times 10^6\ s^{-1}$	k_{10}	$5 \times 10^6\ M^{-1}\ s^{-1}$
k_{11}	$0.23\ s^{-1}$	k_{12}	$150\ s^{-1}$
k_{13}	$623\ s^{-1}$	k_{14}	$2.0 \times 10^8\ M^{-1}\ s^{-1}$

[a] Rate constants for the binding of NADPH (k_1–k_4) and of $NADP^+$ (k_{11}–k_{14}) were estimated by progress curve analysis and were fixed in all simulations. The ratio of k_9 to k_{10} was fixed at 0.2 M equal to $K_{xylitol}$. Eight progress curves, four forward and four reverse reactions, were used for these simulations. Standard errors were 20% or better. [b] Values given in parentheses are for NADPD. Actual progress curves were used to estimate k_{7D}, while k_{8D} was calculated as $k_{8D} = k_{8H}{}^{D}K_{eq}/{}^{D}k_7$ (see text for details). The values of k_5–k_7 provided the best overall fits for both the NADPH and NADPD progress curve data sets. [c] When the xylose concentration is corrected for the 0.02% level of free carbonyl form (Hayward & Angyal, 1977), $k_5 = 1.1 \times 10^6\ M^{-1}\ s^{-1}$.

Table 4: Comparison of Calculated and Measured Kinetic Parameters for hAR

parameter	calcd	measured[a]
$V_{xylose}/E_t\ (s^{-1})$	0.19	0.20 ± 0.01
$K_{NADPH}\ (\mu M)$	0.005	<0.10
K_{xylose} (mM)	1.0	1.5 ± 0.1
$K_{i\ NADPH}\ (\mu M)$	0.013	0.010[b]
$K_{d\ NADPH}\ (\mu M)$	1.5	
$V_{xylitol}/E_t\ (s^{-1})$	0.08	0.05 ± 0.01
$K_{NADP^+}\ (\mu M)$	0.003	<0.10
$K_{xylitol}$ (mM)	160	150 ± 20
$K_{i\ NADP^+}\ (\mu M)$	0.005	0.006[b]
$K_{d\ NADP^+}\ (\mu M)$	3.1	

[a] Determined by initial velocity studies in 33 mM phosphate buffer (pH 8.0) at 25 °C. [b] Determined by fluorescence titration in 5 mM phosphate buffer (pH 7.0) at 20 °C (Ehrig et al., 1994).

aldehyde (Kormann et al., 1972), and D-xylose (Moonsammy & Stewart, 1961).

DISCUSSION

The crystal structure and catalytic mechanism of aldose reductase have been recently elucidated. The enzyme is an α/β barrel protein (Rondeau et al., 1992) with the NADPH cofactor lying across the lip of the active site pocket at the C-terminal end of the barrel, and almost completely enfolded by a loop of residues (Wilson et al., 1992; Harrison et al., 1994) which leaves only the C4-portion of the nicotinamide ring and the 2′-phosphate of the adenosine ribose exposed to the solvent. The 4-*pro-R* hydrogen of NADPH is exposed at the bottom of a deep active site pocket lined with hydrophobic residues, some of which are contributed by the loop enfolding the reduced nucleotide. In the *E·$NADP^+$ complex, two residues, His110 and Tyr48, along with C4 of the positively charged nicotinamide ring form an anion binding site at the bottom of the active site pocket (Harrison et al., 1994). This site binds anions such as citrate, cacodylate, phosphate, and a variety of negatively charged aldose reductase inhibitors (Ehrig et al., 1994). His110 has been shown to affect the substrate stereochemical selectivity, and Tyr48 to serve as the general acid–base catalyst in the reduction mechanism (Bohren et al., 1994). An adjoining Asp43/Lys77 residue pair underlies and interacts with the phenolic hydroxyl of Tyr48, imparting to it a lower pK_a. The catalytic mechanism of aldose reductase involves access of the carbonyl-containing substrate to the active site pocket of the *E·NADPH complex with subsequent hydride transfer from the 4-*pro-R* position of the 1,4-dihydronicotinamide ring. A proton donated by Tyr48 to the carbonyl oxygen completes the conversion of aldehyde to alcohol.

Kinetic Transients and Isotope Effects. Substrate and solvent deuterium isotope effects determined by steady-state kinetic methods have indicated that both hydride and proton transfer contribute significantly to the rate limitation of the catalytic sequence for hAR (Bohren et al., 1994). However, cofactor exchange with its attendant obligatory loop movement and enzyme conformational change appears to be the rate-limiting step for the overall enzymatic reaction in the direction of aldehyde reduction (Grimshaw et al., 1990b; Grimshaw, 1990; Kubiseski et al., 1992). Kinetic transients detected by stopped-flow methods and reported herein for xylose reduction with NADPH or NADPD and for xylitol oxidation with $NADP^+$ confirm and extend these earlier observations.

The detection of a pre-steady-state burst of product formation and likewise of a primary deuterium isotope effect on either the burst rate or the subsequent steady-state rate is diagnostic for the location of the rate-limiting step(s) in the reaction mechanism. Analysis of both the pre-steady-state kinetic transients and the steady-state reaction progress curves as a function of D-xylose concentration can further establish the relative contribution of the hydride transfer step itself. Thus, in the forward reaction, transient reduction of D-xylose catalyzed by wild-type hAR displays burst kinetics with the rapid formation of 0.99 equiv of enzyme-bound $NADP^+$, followed by a linear steady-state rate of $NADP^+$ production (Figure 3). The observation of burst kinetics requires that there be a slow step following hydride transfer. Moreover, because the pre-steady-state burst is nearly stoichiometric, this step must be *significantly* slower than the hydride transfer step.

When NADPD is used in place of NADPH, a large primary deuterium isotope effect is observed on the burst rate, but not on the final steady-state rate of $NADP^+$ production, provided the concentration of xylose is saturating (Figure 3). Single turnover reactions (Figure 2) also display a deuterium isotope effect on the maximal rate comparable to that for the pre-steady-state burst (Table 2), indicating that hydride transfer itself must be largely rate-limiting for the transient reduction of xylose. Taken together, these facts are consistent with the slowest overall step in the direction of aldehyde reduction being the conformational change (*E·$NADP^+$ → E·$NADP^+$) which precedes and allows $NADP^+$ release, but with hydride transfer largely controlling the pre-steady-state transient rate.

In the direction of xylitol oxidation, the situation is quite different since we do not observe any burst of NADPH formation by stopped-flow and only a linear rate of NADPH production equal to that determined by conventional steady-state kinetic methods. Thus, either hydride transfer itself or some step(s) prior to hydride transfer must limit the overall rate of reaction in this direction. Our laboratory (Grimshaw and Lai, unpublished) and Liu et al. (1993) have observed large primary deuterium isotope effects on both $V_{alcohol}/E_t$ and $V/K_{alcohol}E_t$ when [2-$^2H_2$]benzyl alcohol is used as the alcohol substrate, consistent with hydride transfer being largely rate-limiting for the reverse reaction. As we will

show, the rate for hydride transfer from the xylitol to $NADP^+$ catalyzed by hAR is *unusually* slow for an NAD(P)-dependent dehydrogenase. The conformational change that precedes and allows release of the nucleotide product in the reverse reaction (*E·NADPH → E·NADPH) is also quite slow, but since the hydride transfer rate is so poor for alcohol oxidation, NADPH release contributes only about 15% to the overall rate limitation in the reverse reaction. The importance of these factors will become apparent as we compare and contrast the unique kinetic properties of hAR with those of the C298A mutant hAR in the following paper (Grimshaw et al., 1995a) and those of liver alcohol dehydrogenase (LADH) and lactate dehydrogenase (LDH) in the following discussion.

The relative magnitude of the isotope effects shown in Table 2 can best be understood by considering how individual rate constants in the form of ratios or "commitment factors" (Cook & Cleland, 1981) combine to yield an experimentally observed isotope effect that is smaller than the intrinsic isotope effect on the hydride transfer step itself ($^Dk_7 = k_{7H}/k_{7D}$). (Derivations for each of the equations to be discussed are outlined in the supporting information section.) For example, the isotope effect on the maximum rate constant for transient reduction of xylose ($^Dk_{trans}$) is given by:

$$^Dk_{trans} = (^Dk_7 + (k_{7H}/k_3))/(1.0 + k_{7H}/k_3) \quad (6)$$

where (k_{7H}/k_3) is the sole commitment factor. In principle, each of the steps in the direction of xylose reduction up to and including k_9 for xylitol release should contribute to the expression in eq 6 (Northrop, 1977; Cook & Cleland, 1981). However, because NADPH and xylose are saturating and the step corresponding to k_9 is essentially irreversible in the absence of alcohol product, only k_3 acts to reduce the expression of $^Dk_7$ to the observed value of $^Dk_{trans}$. Substituting the rate constants from Table 3 into eq 6 with $^Dk_7 = (k_{7H}/k_{7D}) = 6.5$[8] and $(k_{7H}/k_3) = 1.46$, we calculate that $^Dk_{trans} = 3.23$, in good agreement with the $^Dk_{trans}$ and $^Dk_{burst}$ values measured in single and multiple turnover experiments, respectively (Table 2).

The commitment factors are more complex for the isotope effect on the maximum turnover rate in the steady state. Thus, for $^DV_{xylose}$, we have:

$$^DV_{xylose} = (^Dk_7 + C_{Vf} + C_r{}^DK_{eq})/(1.0 + C_{Vf} + C_r) \quad (7)$$

where the commitments are now $C_{Vf} \cong k_{7H}/k_{11}$ (see supporting information) and $C_r = k_{8H}/k_9$, and where $^DK_{eq} = 0.93$ is the equilibrium isotope effect on the NAD(P)H-linked reduction of an aldehyde (Cook et al., 1980). Substituting the rate constants from Table 3 into eq 7 we see that $C_{Vf} \cong 565$ is the major factor responsible for reducing $^Dk_7 = 6.5$ to the observed value of $^DV_{xylose} \leq 1.01$. In other words, because k_{11} is rate-limiting for the overall reaction, we find no significant isotope effect on V_{xylose}/E_t.

In the first-order region of the saturation curve, both pre-steady-state transient and steady-state reaction rates are directly proportional to the concentration of D-xylose, and expression of the kinetic isotope effect is controlled by a different set of commitment factors. Thus, $^DV/K_{xylose}$ is given by:

$$^DV/K_{xylose} = (^Dk_7 + C_f + C_r{}^DK_{eq})/(1.0 + C_f + C_r) \quad (8)$$

where the forward commitment factor becomes $C_f = k_{7H}/k_6$, and $C_r = k_{8H}/k_9$ remains the same as in eq 7. In this case, because $C_f = 5.2$ is not nearly as large as C_{Vf}, the net result is a calculated value of $^DV/K_{xylose} = 1.89$, which is again close to the experimentally observed value of 1.82 and 2.2 determined from steady-state rate measurements (Table 2). The same expression (eq 8) is valid for $^D(k_{burst}/K_{xylose})$ and $^D(k_{trans}/K_{xylose})$, and as shown in Table 2, these experimental values are also in accord with the calculated value. Because the reverse hydride transfer rate is so low ($k_{8H} = 0.6\ s^{-1}$), the reverse commitment factor, $C_r = k_{8H}/k_9 \cong 0$, does not contribute significantly in either eq 7 or eq 8. The C_f ratio, or "stickiness" (Cleland, 1977) of xylose, also affects the appearance of the pH profile for V/K_{xylose}, as we will show in our pH studies (Grimshaw et al., 1995b).

Nucleotide Binding-Induced Conformational Change. The large conformational change induced by nucleotide binding to hAR is one key to the unique catalytic properties of hAR. Using stopped-flow methods, we have now established that binding of both NADPH and $NADP^+$ occurs by a two-step process, with rapid formation of a "weak" initial E·Nucl complex followed by a much slower conversion to a "tight" final *E·Nucl complex, which is then competent to bind substrate and catalyze hydride transfer. It is the latter process which presumably involves movement of the nucleotide enfolding loop from the "open" position seen in the apoenzyme structure (Rondeau et al., 1992) to the "closed" position seen in all the AR crystal structures containing bound NADP(H) (Wilson et al., 1992, 1993; Borhani et al., 1992; Harrison et al., 1994; Bohren et al., 1994). Analogous conformational changes involving binary E·Nucl complexes have previously been detected by kinetic methods for a number of NAD(P)-dependent dehydrogenases, notably LADH (Sekhar & Plapp, 1988) and alanine dehydrogenase (AlaDH; Grimshaw et al., 1980). What is surprising about the hAR results is the magnitude of the binding enhancement that occurs on going from the weak to the tight complex. For hAR, this "clamping" effect results in a 100- to 650-fold increase in binding affinity, with resultant K_i values for NADPH (13 nM) and $NADP^+$ (6 nM) that are among the lowest known for NAD(P)-dependent enzymes. By comparison, a 4-fold tightening occurs upon NAD^+ binding to LADH (Sekhar & Plapp, 1988, 1990), and a 50-fold tightening occurs when methotrexate binds to the binary E·dihydrofolate complex of human dihydrofolate reductase (Appleman et al., 1988).

When one compares the rate constants for the hAR clamping step with the corresponding rate constants determined for LADH and AlaDH, the main difference appears to be in the "opening" reaction. For example, isomerization to the tight *E·NAD^+ complex for AlaDH occurs at 72 s^{-1}, while the reverse "opening" reaction has a rate constant of >1000 s^{-1} (Grimshaw & Cleland, 1980). For equine LADH at pH 8, the conformational change to form a tight *E·NAD^+ complex occurs at 620 s^{-1}, and the opening rate is about 10-fold slower at 64 s^{-1} (Sekhar & Plapp, 1990). Thus, each of these "closing" reactions occurs with a rate constant in the 10^2-10^3 range, similar to what we see for hAR ($k_3 \cong k_{12}$

[8] Given the magnitude of $^Dk_7 = 6.5$, this is likely the intrinsic primary deuterium isotope effect for wild-type hAR-catalyzed hydride transfer from NADPH to D-xylose (Scharschmidt et al., 1984).

$\cong 100\ s^{-1}$). It is the very slow "opening" reaction for hAR ($k_4 \cong k_{11} \cong 0.5\ s^{-1}$) which leads to the extremely low K_i values for both $NADP^+$ and NADPH (Table 1). We ascribe this effect to an enhanced stability of the "closed" configuration of the enfolding loop, which, as we will show in the following paper (Grimshaw et al., 1995a), is derived in part from some as yet unidentified interaction(s) with the Cys298 residue located near the enzyme active site.

The nucleotide binding results reported for porcine AR by Kubiseski et al. (1992) are in qualitative, but not quantitative agreement with our results for the human enzyme. Thus, the rate constant (k_{11}) for the $*E{\cdot}NADP^+ \rightarrow E{\cdot}NADP^+$ step which controls turnover in the aldehyde reduction direction is equivalent for porcine ($0.25\ s^{-1}$) and human ($0.23\ s^{-1}$) AR. Also, in the reverse reaction, the $*E{\cdot}NADPH \rightarrow E{\cdot}NADPH$ step for porcine AR was found to be faster than $V_{alcohol}/E_t$, and therefore not rate-limiting for turnover in the direction of alcohol oxidation. However, each of our remaining rate constants (k_1-k_3 and $k_{12}-k_{14}$) are 12- to 150-fold greater than those reported for porcine AR. The difference in buffer concentration (100 mM vs 33 mM) or pH (7 vs 8) between the two sets of experiments may be a factor. However, the major discrepancy appears to result from a difference in the nucleotide concentration dependence of the observed transient reaction rates. As shown in Figure 1, saturation kinetics for human AR only become apparent for NADP(H) concentrations above 10 μM, well above the maximum 8 μM nucleotide concentration employed in the study of Kubiseski et al. (1992). Thus, in order to define the remaining rate constants, these authors had to rely on the concentration dependence of a rather poorly defined "slow second phase" in their fluorescence quenching progress curves. The clear demonstration of saturation kinetics under our experimental conditions, on the other hand, has allowed us to utilize eq 5 to accurately model the progress curves for binding of both NADPH and $NADP^+$ to the human enzyme.

Hydride Transfer. If one compares the actual rate constants for hydride transfer for hAR, LDH, and LADH, the results are quite revealing. Hydride transfer from NAD(P)H to the carbonyl-containing substrate occurs with a rate constant in the $100-1000\ s^{-1}$ range for all three enzymes. Hydride transfer from alcohol to $NAD(P)^+$, however, drops from a value $>750\ s^{-1}$ for LDH (Clarke et al., 1986) or $>500\ s^{-1}$ for LADH (Sekhar & Plapp, 1990) to less $0.6\ s^{-1}$ for hAR. The net result for hAR is a bound-state equilibrium constant that greatly favors the bound alcohol product. At pH 8, the bound-state K_{eq} can be calculated as $k_7/k_8 = 217$ (Table 3). At present, we do not know whether the poor alcohol dehydrogenase activity of hAR is due to an inherent stabilization of the oxidized relative to the reduced form of the bound cofactor, thus disfavoring hydride transfer from the alcohol substrate, or rather to a predisposition of the unique configuration of active site residues, which includes Tyr48, His110, Lys77, and Asp43, toward carbonyl reduction as opposed to alcohol oxidation. Because NAD(P)H-dependent reduction of an aldehyde to an alcohol is the thermodynamically preferred direction, another distinct possibility is that hAR has simply not evolved any mechanism, conformational, chemical, or otherwise, to selectively *enhance* the rate of alcohol oxidation, but merely facilitates the overall reaction without inducing a significant change in the bound-state K_{eq} relative to the external K_{eq} value for the reaction in solution.

The important point is that hAR displays roughly the same catalytic ability in terms of hydride transfer rate to a carbonyl moiety as does LDH, without apparently having to rely on specific interactions with the carbonyl-containing substrate. For hAR, *p*-chlorobenzaldehyde, glyceraldehyde, and xylose are all reduced with approximately the same V/KE_t value, once one corrects for the amount of free aldehyde present in solution (Grimshaw, 1991, 1992). We would ascribe this to the fact that the binary $*E{\cdot}NADPH$ complex generated by conformational clamping has the ability to facilitate hydride transfer to a number of RCHO compounds. The LDH active site, however, only becomes catalytically competent when the specific substrate, pyruvate, binds and induces movement of the flexible protein loop to close down, seal off the active site from solvent, and place Arg109 in the correct alignment to help polarize the substrate carbonyl moiety (Clarke et al., 1988). Taken together, these observations support the contention that the purpose for hAR's extremely tight nucleotide binding is to generate a highly reactive, and thus nonselective, $*E{\cdot}NADPH$ complex capable of efficiently reducing virtually any aldehyde-containing substrate.

Practical Aspects of the Kinetic Model. The complete kinetic model for hAR (Table 3) establishes which enzyme complexes should predominate during steady-state turnover in either reaction direction. Thus, at saturating levels of D-xylose and NADPH, the net rate constant (Cleland, 1975) for the conformational change that precedes the release of $NADP^-$ ($k_{11}' = k_{11}k_{13}/(k_{12} + k_{13}) = 0.19\ s^{-1}$) indicates that this is by far the slowest step, and $*E{\bullet}NADP^+$ should comprise more than 99% of E_t in the steady state. In the direction of xylitol oxidation, the net rate constant for hydride transfer ($k_8' = k_6k_8/(k_6 + k_7) = 0.097\ s^{-1}$) corresponds to the slowest step, so that $*E{\cdot}NADP^+{\cdot}RCH_2OH$ comprises nearly 85% of the total enzyme at saturating levels of xylitol and $NADP^+$. Because the next slowest step in this direction is the conformational change which precedes NADPH release ($k_4' = 0.55\ s^{-1}$), most of the remaining 15% of E_t will be present as the $*E{\cdot}NADPH$ complex in the steady state.

Several predictions follow directly from the kinetic model. Thus, an aldose reductase inhibitor (ARI) that only combines with $*E{\cdot}NADP^+$ should show a K_{ii} value for uncompetitive inhibition versus xylose equal to the K_{is} value for competitive inhibition versus xylitol, since both K_i values are equal to the dissociation constant for ARI binding to the same complex. Such is the case for Sorbinil inhibition of the C298A mutant enzyme (Grimshaw et al., 1995b). Alternatively, an inhibitor that combines with either $*E{\cdot}NADPH$ or $*E{\cdot}NADP^+$, and thus shows noncompetitive inhibition versus xylose, might still display competitive inhibition versus xylitol in the reverse reaction, since only 15% of E_t will be present in the correct form to give a detectable intercept effect. V/E_t for aldehyde reduction should be independent of the substrate identity since the rate-limiting step occurs after the alcohol product has departed, and this has previously been confirmed in several laboratories (Grimshaw et al., 1989; Bohren et al., 1991). Also, because hydride transfer is largely rate-limiting in the reverse reaction, V/E_t for alcohol oxidation may be expected to vary with the alcohol substrate, provided the partitioning ratio (k_7/k_6) does

not also change with the alcohol substrate such that the net rate constant $k_8' = k_8/(1.0 + k_7/k_6)$ remains constant.

Finally, a practical note on the tendency to use K_m values to denote "binding affinity" for a given substrate or for a given mutant enzyme. Using the mechanism shown in Scheme 1, the following expression was derived for K_b, the Michaelis constant for D-xylose (see supporting information):

$$K_b = [k_3k_{11}k_{13}(k_6k_8 + k_6k_9 + k_7k_9)(1.0 + (k_4/k_3))]/ [k_3k_5k_7k_9(k_{11} + k_{12} + k_{13}) + k_3k_5k_{11}k_{13}(k_7 + k_8 + k_9) + k_5k_7k_9k_{11}k_{13}] \quad (9)$$

As one can readily see, this expression bears little resemblance to the ratio (k_6/k_5) that reflects the true "binding affinity" of D-xylose for the *E·NADPH complex. In fact, because k_{11} is so small, the first term in the denominator of eq 9 dominates and the value of K_{xylose} calculated by substituting the rate constants from Table 3 into eq 9 is roughly equal to $k_{11}/k_5 \cong 1.0$ mM. Yet, the ratio $k_6/k_5 = 110$ mM! Thus, only the on-rate (k_5) for aldehyde binding makes a significant contribution, and changes in the off-rate (k_6) will not be reflected in the observed K_{xylose} value. On the other hand, since hydride transfer is largely rate-limiting in the reverse reaction, the $K_{xylitol}$ value (169 mM) is similar to the dissociation constant for xylitol ($k_9/k_{10} = 200$ mM).

Changes in the rate constant for hydride transfer (k_7) or the conformational change that controls $NADP^+$ exchange (k_{11}) can also markedly affect the observed K_{xylose} value. For wild-type hAR we have noted that $K_{xylose} \cong k_{11}/k_5$ and that $k_7/k_{11} \cong 565$. Now, suppose k_{11} were to increase as a result of a site-directed mutagenesis experiment. As k_{11} increases, the numerator of eq 9 increases in direct proportion and the second and third terms in the denominator of eq 9 also begin to contribute. At the point where $k_{11} \cong k_7 = 130\ s^{-1}$, the calculated value of $K_{xylose} \cong 180$ mM! Thus, the "apparent K_m" for D-xylose would have increased roughly 180-fold without any change in the true dissociation constant, $K_{d\ xylose} = k_6/k_5$. Alternatively, if the rate constant for hydride transfer (k_7) were to decrease due to a different point mutation, then by the same reasoning at the point where $k_7 \cong k_{11} = 0.23\ s^{-1}$, then $K_{xylose} \cong 50$ mM. Again, the "apparent K_m" for D-xylose would show a 50-fold increase without any real change in the binding affinity. This type of effect may be relevant to the results reported for several AR mutants (e.g., D43N; Tarle et al., 1993) where $NADP^+$ and NADPH bind with high affinity (k_{11} unchanged), but catalysis has slowed to the point where hydride transfer has likely become rate-limiting (k_7 decreased >565-fold). Thus, caution should be exercised in ascribing large increases in the K_m value for the aldehyde substrate to a decrease in binding affinity (K_d), when a large portion of the observed increase may result from changes in the extent of rate limitation of steps in the reaction mechanism that are not involved with substrate binding.

These stopped-flow studies provide a kinetic model and a set of rate constants which quantitatively describe the hitherto identifiable steps in the overall reaction mechanism. It thus becomes possible to probe the enzymatic mechanism by establishing which steps are affected by specific amino acid mutations. Since the appreciation of the significance of aldose reductase in health and disease continues to be problematic, such site-directed mutagenesis studies and identification of their sites of action within the overall reaction scheme should enable a better understanding of the biology of this enzyme. For instance, we now have the opportunity to better understand the molecular basis for the observed multiple oxidized forms of tissue enzyme activity which are reproduced *in vitro* with thiol-induced variations in aldose reductase activity. Similarly, the role of such parameters as variations in enzyme activity among animal species, enzyme turnover rates, enzyme levels, and inhibitor binding and potency can now be probed by a combination of site-directed mutagenesis and stopped-flow studies based on this kinetic model.

ACKNOWLEDGMENT

The authors thank Dr. Bryce V. Plapp and the members of his laboratory at the University of Iowa, in particular Dr. Keehyuk Kim, for the use of the stopped-flow instrument and for many helpful discussions.

SUPPORTING INFORMATION AVAILABLE

Derivation of expressions for the various kinetic parameters including isotope effects on V/E_t, $V/K_{RCHO}E_t$, and $V/K_{NADPH}E_t$ for an ordered bi-bi kinetic mechanism including isomerization of both the binary E·NADPH and E·$NADP^+$ complexes, as outlined in Scheme 1 (4 pages). Ordering information is given on any current masthead page.

REFERENCES

Appleman, J. R., Prendergast, N., Delcamp, T. J., Freisheim, J. H., & Blakely, R. L. (1988) *J. Biol. Chem. 263*, 10304−10313
Barshop, B. A., Wrenn, R. F., & Frieden, C. (1983) *Anal. Biochem. 130*, 134−145.
Boghosian, R. A., & McGuinness, E. T. (1981) *Int. J. Biochem. 13*, 909−914.
Bohren, K. M., & Gabbay, K. H. (1993) in *Enzymology and Molecular Biology of Carbonyl Metabolism 4* (Weiner, H., Ed.) pp 267−277, Plenum Press, New York.
Bohren, K. M., Page, J. L., Shankar, R., Henry, S. P., & Gabbay, K. H. (1991) *J. Biol. Chem. 266*, 24031−24037.
Bohren, K. M., Grimshaw, C. E., & Gabbay, K. H. (1992) *J. Biol. Chem. 267*, 20965−20970.
Bohren, K. M., Grimshaw, C. E., Lai, C.-J., Harrison, D. A., Ringe, D., Petsko, G. A., & Gabbay, K. H. (1994) *Biochemistry 33*, 2021−2032.
Borhani, D. W., Harter, T. M., & Petrash J. M. (1992) *J. Biol. Chem. 267*, 24841−24847.
Clarke, A. R., Wigley, D. B., Chia, W. N., Barstow, D., Atkinson, T., & Holbrook, J. J. (1986) *Nature (London) 324*, 699−702.
Clarke, A. R., Wilks, H. M., Barstow, D. A., Atkinson, T., Chia, W. N., & Holbrook, J. J. (1988) *Biochemistry 27*, 1617−1622.
Cleland, W. W. (1975) *Biochemistry 14*, 3220−3224.
Cleland, W. W. (1977) *Adv. Enzymol. Relat. Areas Mol. Biol. 45*, 273−388.
Cleland, W. W. (1979) *Methods Enzymol. 63*, 103−138.
Cleland, W. W. (1987) in *Isotopes in Organic Chemistry* (Buncel, E., & Lee, C. C., Eds.) Vol. 7, Chapter 2, Elsevier, Amsterdam.
Cook, P. F., & Cleland, W. W. (1981) *Biochemistry 20*, 1790−1796.
Cook, P. F., Blanchard, J. S., & Cleland, W. W. (1980) *Biochemistry 19*, 4853−4858.
Del Corso, A., Barsacchi, D., Giannessi, M., Tozzi, M. G., Camici, M., & Mura, U. (1989) *J. Biol. Chem. 264*, 17653−17655.
Ehrig, T., Bohren, K. M., Prendergast, F. G., & Gabbay, K. H. (1994) *Biochemistry 33*, 7157−7165.
Gill, S. C., & von Hippel, P. H. (1989) *Anal. Biochem. 182*, 319−326.
Grimshaw, C. E. (1991) *Biochem. Biophys. Res. Commun. 175*, 943−948.
Grimshaw, C. E. (1992) *Biochemistry 31*, 10139−10145.

Grimshaw, C. E., & Cleland, W. W. (1980) *Biochemistry 20*, 5650–5655.
Grimshaw, C. E., & Lai, C.-J. (1995) *Enzymology and Molecular Biology of Carbonyl Metabolism 6* (Weiner, H., Ed.) pp 229–240, Plenum Press, New York.
Grimshaw, C. E., Cook, P. F., & Cleland, W. W. (1980) *Biochemistry 20*, 5655–5661.
Grimshaw, C. E., Shahbaz, M., Jahangiri, G., Putney, C. G., McKercher, S. R., & Mathur, E. J. (1989) *Biochemistry 28*, 5343–5353.
Grimshaw, C. E., Shahbaz, M., & Putney, C. G. (1990a) *Biochemistry 29*, 9936–9946.
Grimshaw, C. E., Shahbaz, M., & Putney, C. G. (1990b) *Biochemistry 29*, 9947–9955.
Grimshaw, C. E., Bohren, K. M., Lai, C.-J., & Gabbay, K. H. (1995a) *Biochemistry 34*, 14366–14373.
Grimshaw, C. E., Bohren, K. M., Lai, C.-J., & Gabbay, K. H. (1995b) *Biochemistry 34*, 14374–14384.
Harrison, D. H., Bohren, K. M., Ringe, D., Petsko, G. A., & Gabbay, K. H. (1994) *Biochemistry 33*, 2011–2020.
Hayward, L. D., & Angyal, S. J. (1977) *Carbohydr. Res. 53*, 13–20.
Kormann, A. W., Hurst, R. O., & Flynn, T. G. (1972) *Biochim. Biophys. Acta 258*, 40–55.
Kubiseski, T. J., Hyndman, D. J., Morjana, N. A., & Flynn, T. G. (1992) *J. Biol. Chem. 267*, 6510–6517.
Liu, S.-Q., Bhatnagar, A., & Srivastava, S. K. (1993) *J. Biol. Chem. 268*, 25494–25499.
Moonsammy, G. I., & Stewart, M. A. (1961) *J. Neurochem. 14*, 1187–1193.
Northrop, D. B. (1977) in *Isotope Effects on Enzyme-Catalyzed Reactions* (Cleland, W. W., O'Leary, M. H., & Northrop, D. B., Eds.) pp 122–152, University Park Press, Baltimore.
Robinson, W. G. (1966) *Methods Enzymol. 9*, 332–336.
Rondeau, J.-M., Tête-Favier, F., Podjarny, A., Reymann, J.-M., Barth, P., Biellmann, J.-F., & Moras, D. (1992) *Nature 355*, 469–472.
Ryle, C. M., & Tipton, K. F. (1985) *Biochem. J. 277*, 621–627.
Sato, S., & $K_a$dor, P. F. (1990) *Biochem. Pharmacol. 40*, 1033–1042.
Scharschmidt, M., Fisher, M. A., & Cleland, W. W. (1984) *Biochemistry 23*, 5471–5478.
Sekhar, V. C., & Plapp, B. V. (1988) *Biochemistry 27*, 5082–5088.
Sekhar, V. C., & Plapp, B. V. (1990) *Biochemistry 29*, 4289–4295.
Srivastava, S. K., Hair, G. A., & Das, B. (1985) *Proc. Natl. Acad. Sci. U.S.A. 82*, 7222–7226.
Tanimoto, T., Fukuda, H., Yamaha, T., & Tanaka, C. (1986) *Chem. Pharm. Bull. (Jpn.) 34*, 4183–4189.
Tarle, I., Borhani, D. W., Wilson, D. K., Quiochol, F. A., & Petrash, J. M. (1993) *J. Biol. Chem. 268*, 25687–25693.
Vander Jagt, D. L., & Hunsaker, L. A. (1993) *Enzymology and Molecular Biology of Carbonyl Metabolism 4* (Weiner, H., Ed.) pp 279–288, Plenum Press, New York.
Wermuth, B., Bürgisser, H., Bohren, K., & Von Wartburg, J.-P. (1982) *Eur. J. Biochem. 127*, 279–284.
Wilkinson, G. N. (1961) *Biochem. J. 80*, 324–332.
Wilson, D. K., Bohren, K. M., Gabbay, K. H., & Quiocho, F. A. (1992) *Science 257*, 81–84.
Wilson, D. K., Tarle, I., Petrash, J. M., & Quiocho, F. A. (1993) *Proc. Natl. Acad. Sci. U.S.A. 90*, 9847–9851.
Zimmerle, C. T., Patane, K., & Frieden, C. (1987) *Biochemistry 26*, 6545–6552.

BI950555K